AJChE 2017, Vol. 17, No. 1, 29 – 36

# Molecular Dynamics Simulation of the Nano-scale Solutal Marangoni Convection

***Yosuke Imai* [*,1]**
***Takuya Yamamoto* [2]**
***Yasunori Okano* [1]**
***Ryuma Sato* [3]**
***Yasuteru Shigeta* [3]**

[1] *Department of Materials Engineering Science, Osaka University, Machikaneyama 1-3, Toyonaka, Osaka 563-8531, Japan*

[2] *Department of Frontier Science for Advanced Environment, Tohoku University, 6-6-02 Aza Aoba, Aramaki, Aoba-ku, Sendai, Miyagi 980-8579, Japan*

[3] *Center for Computational Sciences, University of Tsukuba, 1-1-1 Tennodai, Tsukuba, Ibaraki 305-8577, Japan*

[*] *e-mail:* y-imai@cheng.es.osaka-u.ac.jp

Non-equilibrium molecular dynamics simulations for the 2- and 3-phase systems were performed to investigate the flow with two free surfaces in a nanoscale, where solute, water, and argon were assigned as each phase. We observed that the behaviors of some 3-phase systems significantly differ from those of 2-phase systems. In all 2-phase systems, the solutes just diffused into the water phase. On the other hand, the solutes were transferred along the liquid-gas interfaces in the case of 3-phase systems with a large surface tension gradient. These results indicated that solutal Marangoni convection existed even in the nano-scale and it affected mass transfer greatly.

**Keywords:** non-equilibrium molecular dynamics, concentration gradient, Marangoni convection, liquid film, flow fields, nano-scale

## INTRODUCTION

Marangoni convection is driven by a surface tension gradient, and it is one of the most important factors to understand flow structures in multiphase systems such as a semiconductor crystal growth (Hirata 2007). The surface tension gradient is typically caused by a temperature and/or a concentration gradient along a free surface. Especially, the Marangoni convection induced by the concentration gradient is called "solutal Marangoni convection". The Marangoni convection has been well investigated in a macro-scale environment to improve processes of the crystal growth. In recent years, the Marangoni convection has been remarked not only in the macro-scale, but also in the nano-scale for applications of a focused ion beam milling (Das *et al*. 2015) and a fluid evaporating system (Sumith *et al*. 2016). Surface forces such as surface tension become more dominant than body forces such as gravitational force, because a specific surface area of an

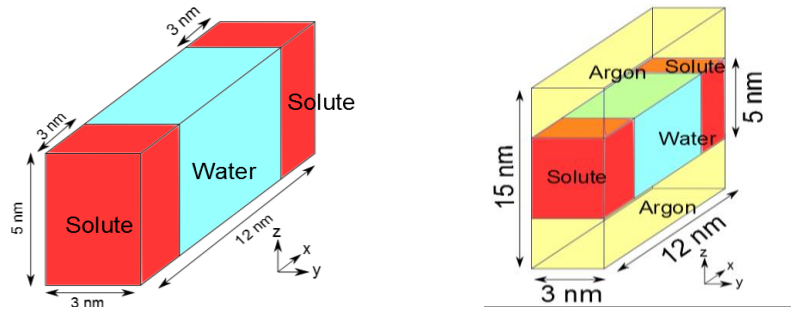


**Fig. 1:** Numerical configurations: (a) 2-phase system which consists of water and solute and (b) 3-phase system which consists of water, solute and argon.

object is large in the nano-scale. Therfore, understanding of the nano-scale Marangoni convection is very important for predicting the nano-scale fluid behavior. However, only a few researches about the nano-scale Marangoni convections have been conducted so far. This is because experimental observation of the flow in the nano-scale is very difficult and a continuum assumption, which is commonly used for calculating a macroscopic Marangoni convection, breaks down in the nano-scale. Because the continuum assumption ignores intermolecular effects, it is not able to describe fluid behavior exactly in the nano-scale where the intermolecular effects become larger. One example for the differences was reported by Holt and co-workers. They measured a mass transfer rate of gas and water into a hole of a membrane made from carbon nanotube by using Computational Fluid Dynamics (CFD) simulation (Holt *et al.* 2006). They reported that the mass transfer rates in the nano-scale calculated by CFD differed greatly from actual values. Therfore it is essential for understanding nano-scale flow phenomenon at an atomic-level by using a Molecular Dynamics (MD) simulation.

To the best of our knowledge, though a few researches about a nano-scale Marangoni convection caused by a temperature gradient were conducted (Das *et al.* 2015, Maier *et al.* 2012, Murata *et al.* 2006, Sumith *et al.* 2016), no paper has been theoretically reported about the nano-scale solutal Marangoni convection. Therfore, we here focused on the nano-scale solutal Marangoni convection. In this work, we performed non-equilibrium MD simulations of the multiphase systems that composed of the solutes, water, and argon by using five kinds of solutes in order to reveal how the solutal Marangoni convection affects the flow and the mass transfer in the nano-scale. In the following section, we explain the model systems and details of numerical simulations. The results and discussion are given in Sec. III. Finally, we conclude in Sec. IV.

## NUMERICAL METHODS

### System

We here considered two systems: one consists of water and solute, and the other consists of water, argon, and solute, which have two liquid-gas interfaces as illustrated in **Figure 1**. Hereafter, we refer them to the 2- and 3-phase systems,

**Table 1.** Number of each molecule

| | Solute | Water | Total |
|---|---|---|---|
| **Ethylamine** | 874 | 3079 | 3953 (3963) |
| **Methanol** | 1420 | 3073 | 4493 (4503) |
| **Formic acid** | 1376 | 2716 | 4092 (4102) |
| **Ethylenediamine** | 784 | 2765 | 3549 (3559) |
| **Formamide** | 1286 | 2778 | 4064 (4074) |

respectively. By comparing the 2-phase system with the 3-phase one, effects of free surfaces on the solutes transfer was investigated. Five kinds of solutes (Ethylamine, Methanol, Formic acid, Ethylenediamine and Formamide), which have different surface tension each other, were utilized in this study. The 2-phase (3-phase) system was initially set as a rectangular box with the lengths of 12 nm, 3 nm, and 5 (15) nm along the *x*-, *y*- and *z*-directions, respectively. The total numbers of the molecules in the systems are summarized in **Table 1**. Note here that the number of argon molecules was set to 10 in all 3-phase system and the numbers in the parentheses represent the total number of molecules in each of the 3-phase system. To reduce calculation cost, we set the *y*-direction as short as possible, satisfying a length limit which has to set more than twice as long as cut-off radius which is set to 1.2 nm in all simulations.

**Molecular Dynamics (MD) Simulation**

We performed non-equilibrium molecular dynamics simulations by means of GROMACS package software (Abraham *et al*. 2014). Velocity Verlet method was used to integrate Newton's equation of motion with 2 fs time step. Gromos53a6 (Oostenbrink *et al*. 2004) and SPC/E model (Berendsen *et al*. 1987) were adopted for the force field parameters of the solutes and the water, respectively. For both the 2- and 3-phase systems, the 3-dimensional periodic boundary condition was applied. The electrostatic interactions were calculated using the particle mesh Ewald method (Darden *et al*. 1993). To set initial profile of the molecules in the 2- and 3-phase systems, we first performed energy minimization followed by the NVT and NPT ensemble equilibrations for the systems which consist of only solute during 2 ns and 10 ps, respectively. Energy minimization was performed for 113 steps. Berendsen thermostat (Berendsen *et al*. 1984) was used to maintain the system temperature at 300 K during the NVT and NPT ensemble simulations. During the NPT ensemble simulations, we also adopted Berendsen barostat to maintain the system pressure at 1 bar. The same operations were done for the water and the argon. After getting all equilibrated structures of the partial systems, we combined them to construct the systems as illustrated in **Figure 1**. For the case of Ethylamine, all simulations were performed at 280 K to keep liquid phase, because the boiling point of Ethylamine is about 290 K. For production runs, NVT ensemble MD simulations were performed

**Table 2.** Physical properties of each solute (Jasper *et al.* 1972)

| Solute | $\rho$[kg/m$^3$] | $D_{ij}$ [m$^2$/s] | $\gamma_i$ [×10$^{-3}$ N/m] |
|---|---|---|---|
| **Formamide** | 1133 | 1.26 | 56.86 |
| **Ethylenediamine** | 899 | 2.79 | 41.00 |
| **Formic acid** | 1220 | 1.60 | 36.91 |
| **Methanol** | 792 | 2.47 | 21.91 |
| **Ethylamine** | 689 | 4.09 | 20.30 |

for 200 ps without any pre-equilibration, where the Nosé-Hoover thermostat (Martyna *et al*. 1992) was used instead of the Berendsen thermostat. Because the exact velocity data is required to analyze the solutal Marangoni flow in this study, we used Nosé-Hoover thermostat, which always preserves quasi-energy in NVT simulation.

**Mutual Diffusion Coefficient**

To investigate the penetration rate of solutes into the water phase quantitatively, a mutual diffusion coefficient, $D_{ij}$, of the waters for each solute were calculated. For liquid mixture, $D_{ij}$ generally depends on the mixture compositions and the Darken relation postulates (Darken 1948)

$$D_{ij} = x_i D_{j,\text{self}} + x_j D_{i,\text{self}} \quad (1)$$

where $D_{i,self}$ and $x_i$ are self diffusion coefficient and mole fraction of component *i*, respectively. The self diffusion coefficient is determined by mean-square displacement of molecules as

$$D_{i,\text{self}} = \lim_{t\to\infty} \frac{1}{6t} \left\langle \left| \mathbf{r}_i(t) - \mathbf{r}_i(0) \right|^2 \right\rangle \quad (2)$$

where $\mathbf{r}_i(t)$ is the coordinate of molecule of *i* component and $r_i(0)$ is an initial coordinate of *i* component at the time, *t*.

**RESULTS AND DISCUSSION**

**Properties of Each Solute**

The calculated mutual diffusion coefficient $D_{ij}$, experimental density $\rho_i$, and experimental surface tension $\gamma_i$ are listed in **Table 2.** Ethylamine has the largest mutual diffusion coefficient and Formamide has the lowest among five kinds of solutes, respectively. The surface tension of water is about $\gamma_{water}$ = 71.99 × 10$^{-3}$ N/m at 300 K. Ethylamine and Methanol have relatively large surface tension difference compared with that of the water $\Delta\gamma_i = \gamma_i - \gamma_{water}$, while the upper three solutes in **Table 2** have relatively small $\Delta\gamma_i$. According to these values, the solutes used in this study can be roughly categorized into two groups. One has smaller $\Delta\gamma_i$ (**Group 1**: Formamide, Ethylenediamine and Formic acid), and the other has larger $\Delta\gamma_i$ (**Group 2**: Methanol and Ethylamine).

**Concentration Distribution of Solute**

To visualize averaged concentration and velocity in the liquid film, we computed the average of them in each cell with $\Delta x$ =

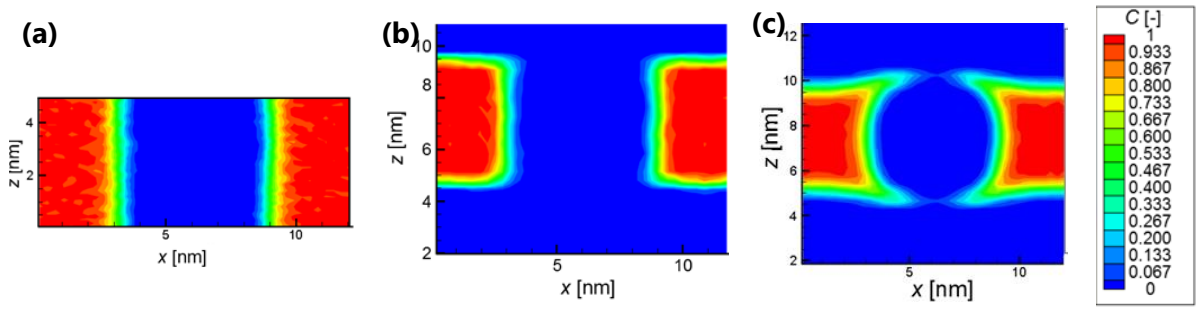


**Fig. 2:** Concentration distributions of the solute: (a) 2-phase system: Methanol (**Group 2**) was used as the solute, (b) 3-phase system: Formamide (**Group 1**) was used as the solute and (c) 3-phase system: Methanol (**Group 2**) was used as the solute.

0.3 and $\Delta z$ = 0.375 nm during 10 ps over 100 runs. In this study, we applied ensemble average not time average to obtain quantitative values because this phenomenon was in an unsteady state.

We first compared the concentration distribution of the 2-phase and 3-phase systems with the five kinds of the solutes. Concentration was defined within a range of 0 to 1. **Figure 2** showed the snapshot of the concentration distribution at 45 ps. In all 2-phase simulations, we observed that the all solutes just diffused into the water phase (**Figure 2 (a)**). In the 3-phase simulations, the behavior of the solutes in **Group 1** is a bit different from that in **Group 2**. In the case of **Group 1**, the solutes just diffused into the water phase as seen in the 2-phase simulations (**Figure 2 (b)**). On the other hand, in the case of **Group 2**, it was observed that some solutes diffused into the water phase and others were also transferred along the liquid-gas interfaces (**Figure 2 (c)**). The solutes moved faster in the 3-phase system with large surface tension difference (**Group 2**) than in the 2-phase system as clearly seen in **Figure 2**. This result indicated that strong flow was developed along the liquid-gas interfaces in the systems with large surface tension difference and the flow promoted the solute transfer.

**Velocity Distribution in the Liquid Film**

We depicted averaged velocities of the cells during 10 ps over 100 runs to observe the flow fields in the liquid film. The velocity distributions mapped onto the *x*-*z* plane at 10 ps and 45 ps are shown in **Figure 3**. In the case of **Group1**, the flow in the liquid film is random, and thus the Marangoni convection was not seen clearly at both 10 ps and 45 ps (**Figure 3 (a)**). The flow fields of **Group 2** were different from those of **Group 1**. The strong flow was generated in the direction toward the expansion of the water phase (**Figure 3 (b)**). After that, four vortices were generated by the strong flow along the interfaces. The maximum velocity of **Group 2** was about 5-6 times larger than that of **Group 1**.

To analyze the velocity fields more quantitatively, we projected the velocity onto the *x* direction along the upper interface and plotted an approximate regression curve of velocity and

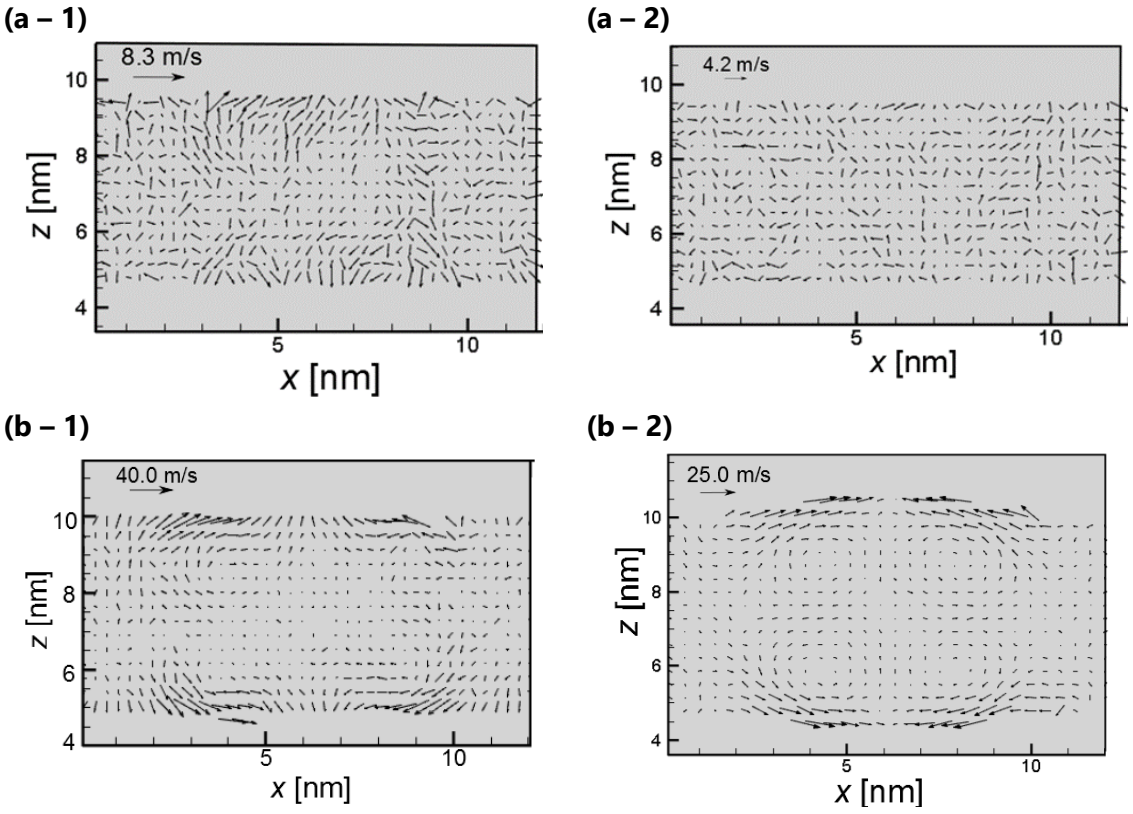


**Fig. 3:** Velocity distributions in the liquid film: (a) 3-phase system: Formamide (**Group 1**) was used as the solute (b) 3-phase system: Methanol (**Group 2**) was used as the solute (1) at 10 ps and (2) at 45 ps.

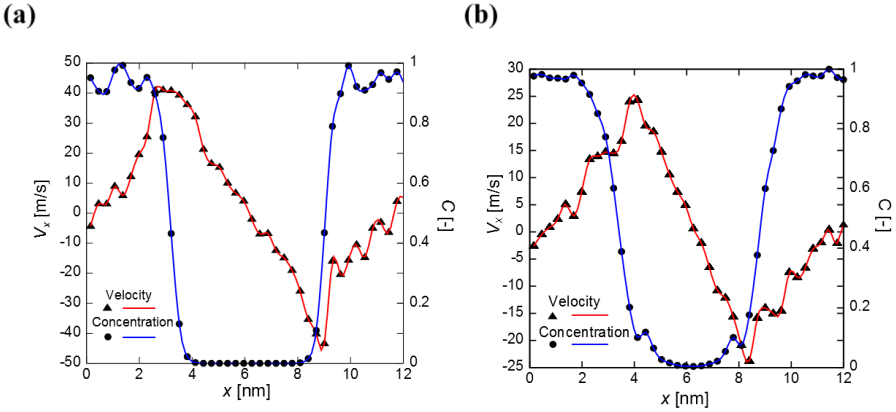


**Fig. 4:** Velocity in the *x* direction at the upper liquid-gas interface along the *x* axis: (a) at 10 ps and (b) at 45 ps in the case of Methanol (**Group 2**). Blue and red lines express the approximate regression curves of the concentration and velocity, respectively.

concentration of the solute as a function of *x* in the case of Methanol (**Figure 4**). The black circle and triangle represent the ensemble averaged concentration and velocity, respectively. The magnitude of the flow velocity is large at where the concentration gradient was steep, and the flow velocity approached zero at where

the concentration gradient was very small. The locations of the maximum velocity and the steepest concentration gradient moved toward the central direction of the film. The reason why the steep concentration gradient moved toward the center of the liquid film is diffusion and convection along the interfaces. These results clearly implied that the flow was considered to be generated due to the concentration gradient and it was found that solutal Marangoni convection existed even in the nano-scale and it promoted the solutes transfer. According to the results of **Group 1**, a lager surface tension difference may be necessary to drive the solutal Marangoni convection than the macro-scale one in the nano-scale.

## CONCLUSION

Non-equilibrium molecular dynamics simulations were performed for the 2- and 3-phase systems in the nano-scale. In the simulations of the 3-phase systems, we observed two ways of solutes being transferred into the water phase. In the cases of solute with small surface tension difference between water and solute, the solute just diffused into the water phase. On the other hand, in the cases of solute with small surface tension difference, the solutes were transferred along liquid-gas interfaces. We also found that four vortices were developed by a strong flow along the liquid-gas interfaces and this strong flow promoted the solute transfer. According to the relation between concentration gradient and velocity, it is considered that the flow was driven by the surface tension gradient due to the concentration gradient of the solute, indicating that the solutal Marangoni convection exists and it promoted the mass transfer even in the nano-scale.

In our future work, we will compare these results with those obtained by CFD simulations and investigate the quantitative differences between nano- and macro-scale Marangoni convection.

## ACKNOWLEDGEMENT

This research is financially supported by a Grant-in-Aid for Challenging Exploratory Research (No. 15K14202) from the Ministry of Education, Culture, Sports, Science and Technology of Japan.

## REFERENCES

1. Abraham, M. J., Van der Spoel, D. Lindahl, E., Hess, B. (2014) The GROMACS development team, GROMACS User Manual version 4.6.5, http://www.gromacs.org/ .
2. Berendsen, H. J. C., Postma, J. P. M., Van Gunsteren, W., Dinola, A. and Haak, J. R. (1984) Molecular dynamics with coupling to an external bath, J. Chem. Phys. 81, 3684.
3. Berendsen, H. J. C., Grigera, J. R. and Straatsma, T. P. (1987) The missing term in effective pair potentials, J. Phys. Chem. 91, 6269.
4. Darken, L. S. (1948) Diffusion, mobility and their interrelation through free energy in binary metallic systems, Trans. Aime., 175, 184.
5. Darden, T., York, D. and Pedersen, L. (1993) Particle mesh Ewald: An

N•log(N) method for Ewald sums in large systems, J. Chem. Phys., 98, 10089.

6. Das, K., Johnson, H. T. and Freund, J. B. (2015) Atomic-scale thermocapillary flow in focused ion beam milling, Phys. Fluids, 27, 052003.
7. Hirata, A. (2007). A united theory for interphase transport phenomena with interfacial velocity and surface tension gradient: application to single crystal growth and microgravity science, Fluid Dyn. Mater. Process, 3, 203.
8. Holt, J. K., Park, H. G., Wang, Y., Stadermann, M., Artyukhin, A.B., Grigoropoulos, C.P., Noy, A. and Bakajin, O. (2006) Fast mass transport through sub-2-nanometer carbon nanotubes, Science, 312, 1034.
9. Jasper, J. J. (1972) The surface Tension of Pure Liquid Compounds, J. Phys. Chem. Ref. Data, 1, 841.
10. Maier, H. A., Bopp, P. A. and Hampe, M. J. (2012) Non-equilibrium molecular dynamics simulation of the thermocapillary effect, Can. J. Chem. Eng., 902, 833.
11. Martyna, G. J., Klein, M. L. and Tuckerman, M., (1992) Nosé-Hoover chains: The canonical ensemble via continuous dynamics, J. Chem. Phys., 97, 2635.
12. Murata, A. and Mochizuki, S. (2006) Molecular dynamics simulation of micro-droplet motion on solid surface induced by temperature gradient, J. Jpn. Soc. Mech. Eng., 72, 987.
13. Oostenbrink, C., Villa, A., Mark, A. and Van Gunsteren, W. (2004) A biomolecular force field based on the free enthalpy of hydration and solvation: The GROMOS force-field parameter sets 53A5 and 53A6, J. Comput. Chem., 25, 1656.
14. Sumith, Y. D. and Maroo, S. C. (2016) Origin of Surface-Driven Passive Liquid Flows, Langmuir, 32, 8593.